Quantum Electronics **47** (10) 942–948 (2017)

https://doi.org/10.1070/QEL16459

Hydrodynamic effects in laser cutting of biological tissue phantoms

V.S. Zhigarkov, V.I. Yusupov, S.I. Tsypina, V.N. Bagratashvili

Abstract. **We study the thermal and transport processes that occur in the course of incision formation at the surface of a biological tissue phantom under the action of near-IR, moderate-power, continuous-wave laser radiation (λ = 1.94 μm) delivered by means of an optical fibre with an absorbing coating on its exit face. It is shown that in addition to the thermal effect, the laser-induced hydrodynamic effects caused by the explosive boiling of the interstitial water make a large contribution to the phantom destruction mechanism. These effects lead to the tissue rupture accompanied by the ejection of part of the fragmented substance from the site of laser impact and the formation of highly porous structure near the incision surface. We have found that the depth, the width and the relief of the laser incision wall in the case of using the optical fibre moving with a constant velocity, depend on the fibre tilt angle with respect to the phantom surface, as well as the direction of the fibre motion.**

Keywords: *laser medical technologies, fibre laser, biotissue cutting, optical fibre, absorbing coating, laser-induced hydrodynamic processes, biotissue phantom.*

1. Introduction

Among a variety of laser applications in medicine, an important role is played by the cutting and thermal destruction of biotissues [1–7]. In recent time the reliable and practical fibre lasers having a moderate power of 1–10 W and generating continuous-wave radiation in the near-IR range find wider and wider application for these purposes [8–10]. One of such applications is based on the formation of laser-induced channels [3, 11, 12] or incisions [13, 14] in a biotissue by moving the face of an optical fibre heated by the laser radiation. The distal face of the fibre is coated with a light-absorbing carbon-containing layer [3, 15–17] or special convertors [18–20] that strongly absorb the laser radiation and provide the heating of the fibre face. The presence of the absorbing coating provides the unified (practically independent of the wavelength) regimes of the impact of the used laser radiation on the biotissue. The use of laser radiation weakly absorbed in the biotissue, allows the laser impact efficiency to be increased and the undesired overheating of the adjacent tissues to be reduced [3, 17]. In contrast to a traditional scalpel, the dissection and removal of biotissues using a fibre laser provides much smaller blood loss [1].

Successful introduction of this approach into wide clinical practice makes it necessary to optimise the process of laser action on the biotissue, and, besides that, to reveal the dominant effects in the laser impact. Thus, the rate of the tissue dissection, the depth, width and quality of the incision are determined by a number of parameters of the process, namely, the laser power, the velocity of the fibre motion and the force pressing the fibre to the tissue. As shown in Refs [17, 20], the parameters of laser incision of a biotissue also essentially depend on the tilt angle of the fibre with respect to the tissue surface.

Considering the key mechanisms of the impact of moderate-power laser radiation on a biotissue, we should note that, besides the heating [4, 7, 13, 20], the processes of boiling in biological fluids can make an essential contribution [21–24], as well as the processes related to the generation and cavitation collapse of vapour-gas bubbles [12, 15], and the excitation of intense acoustic oscillations in a wide range of amplitudes and frequencies [12, 25, 26].

In the present paper, we study the parameters of laser incisions at the surface of biological tissue phantoms at different tilt angles of the fibre with respect to the phantom surface. We show that alongside with the thermal action of laser radiation an important role is played by the laser-induced hydrodynamic processes caused by water boiling.

2. Materials and methods

In the experiment, we used a phantom of cartilage tissue, made of polyacrylamide gel with the linkage degree 1:9 in correspondence with the technique described in Ref. [27]. To prepare the polyacrylamide gel we mixed the solution of acrylamide and bisacrylamide with the weighted portion of ammonium persulphate. The obtained solution was poured into a Petri dish, the layer thickness being ~5 mm. To initiate the polymerisation, a drop of TEMED was added. After the completion of the polymerisation process (accompanied by the gel temperature increase to 60 °C) the obtained phantom plate was taken out from the solution and using a scalpel a 20×30 mm sample was cut from the plate to be used in the experiments. The phantom obtained using this technique possesses the optical properties, the heat conduction and the composition of the interstitial fluid, corresponding well to those of the cartilage tissue [27]. We also performed experi-

V.S. Zhigarkov, S.I. Tsypina, V.N. Bagratashvili Institute of Photon Technologies, Federal Scientific Research Centre 'Crystallography and Photonics', Russian Academy of Sciences, ul. Pionerskaya 2, 108840 Moscow, Troitsk, Russia;
V.I. Yusupov Institute of Photon Technologies, Federal Scientific Research Centre 'Crystallography and Photonics', Russian Academy of Sciences, ul. Pionerskaya 2, 108840 Moscow, Troitsk, Russia; Institute of Applied Physics, Russian Academy of Sciences, ul. Ul'yanova 46, 603950 Nizhnii Novgorod, Russia;
e-mail: iouss@yandex.ru

Received 28 June 2017; revision received 9 August 2017
Kvantovaya Elektronika **47** (10) 942–948 (2017)
Translated by V.L. Derbov

ments with the phantoms of soft tissues. For this purpose, the phantoms were prepared with the addition of hydrolysate of the gel-forming protein collagen having the concentrations 5% and 10%, which increased their flexibility.

The experiments on the laser cutting of the biological tissue phantom were carried out using the setup, comprising a fibre laser and a programmable three-coordinate high-precision positioner. The phantom sample was fixed on the positioner, its surface being fixed horizontal and coincident with the xy plane of the positioner movement. For rigid fixation, the fibre was placed in a steel needle, making the specified tilt angles $\alpha = 90°$ (perpendicular), 60° and 45° with the phantom surface. The working end of the fibre protruded from the needle by a few millimetres and was pressed to the surface of the sample by a calibrated spring with the force 0.1 ± 0.02 N. In the process of cutting, the high-precision positioner with the phantom fixed on it moved with the constant velocity 1 mm s^{-1} along a U-shaped trajectory. At the initial moment of the motion, the laser was switched on automatically. Thanks to the chosen shape of the trajectory for the fibre tilt angles 60° and 45°, the cutting at the initial stage was executed in the direction of the obtuse angle and at the final stage in the direction of the acute angle.

To check the hypothesis of laser-induced hydrodynamic processes, contributing to the mechanism of laser destruction of the phantom polymer material, we collected and analysed the substances, released from the site of laser impact. For this purpose, we executed the phantom cutting with a glass plate placed at the distance of ~5 mm from the phantom surface to collect the expelled products of tissue cutting.

As a source of laser radiation, we used a LS-1.94 moderate-power fibre laser (IRE-Polus, Russia) having a radiation wavelength of 1.94 μm, joined with a silica fibre having a light-guiding core diameter of 400 μm. The absorption coefficient of the radiation with $\lambda = 1.94$ μm in water – the main chromophore of water-filled biotissues in the ICR region – amounts to 92 cm^{-1} [28]. Before the start of phantom cutting, the fibre face was cleaved. Then in order to obtain a stable absorbing coating in the form of a carbon film, the face was pressed to the surface of activated coal through a thin polyethylene film and short-time laser irradiation at a power $P = 3$ W m was executed.

The temperature fields near the fibre face in the process of phantom cutting was studied using a FLIR A655sc thermal imaging camera (Sweden), equipped with a special head to obtain images with 640×480 pixels and a resolution of 17 μm. The camera was installed in the plane, determined by the direction of the steel needle carrying the fibre and the vector of the positioner motion, making an angle of 45° with the phantom surface. To visualise the region of laser incision, we used a PHENOM ProX scanning electron microscope (Phenom World, the Netherlands).

The optical microscopic studies were executed by means of a Micros MC 300 microscope (Micros, Austria) with a luminescence unit equipped with a colour 5-megapixel DCM510 digital camera. To construct the 3D model of the sample surface relief after the laser cutting, we used a Huvitz HRM-300 microscope (Korea) with an objective providing fivefold magnification, equipped with a Huvitz HM-TV0.5XC digital colour camera (Korea). The obtained 3D images were then processed using the MatLab software package. The processing allowed determination of the mean values and the standard deviations of the widths and depths of the incisions, formed on the surface of the phantoms (along the entire length of ~10 mm) at different tilt angles (90°, 60°, 45°) of the fibre without collagen and with collagen having a concentration of 5% and 10%.

3. Obtained results

The formation of a laser channel at the phantom surface occurs in the course of moving the sample surface relative to the immobile fibre with its face heated by the laser radiation. It appeared that the channel parameters, such as depth, width and surface quality (relief) of the incision, essentially depend on the tilt angle of the fibre and the direction of its motion (Fig. 1). Figure 1a shows examples of images of the laser incision at the tissue phantom surface for $\alpha = 45°$ and different directions of motion. From the comparison of the 2D images, one can see that when the fibre is moved along the phantom surface in the direction of the obtuse angle, the width of the channel is greater and the quality of its bottom surface is essentially better (the roughness is smaller). The depth of the laser channel for $\alpha = 90°$ also depends on the direction of motion (Fig. 1b).

When $\alpha = 45°$ and the fibre moves in the direction of the obtuse angle, the depth of the produced channel h is maximal and amounts to 0.5 ± 0.05 mm. When the fibre having the

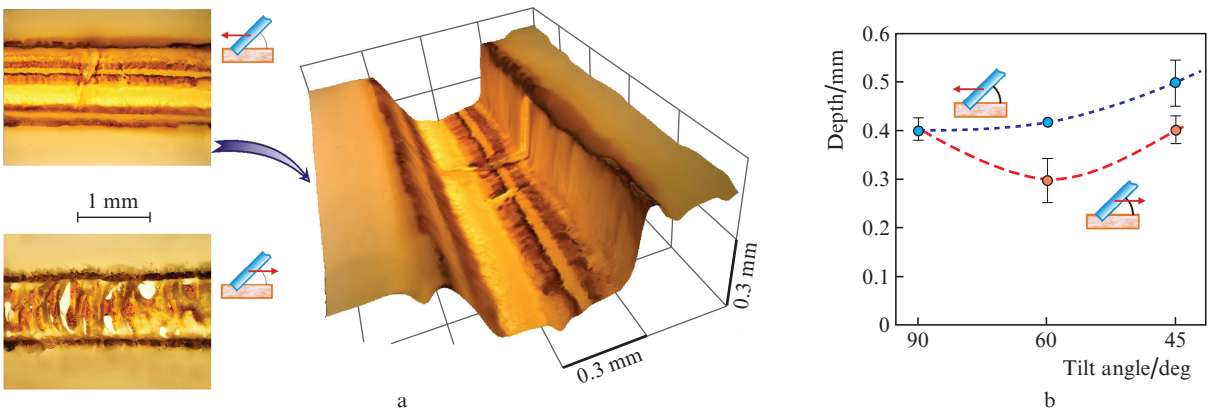

Figure 1. (a) Images of the laser incision at the surface of the tissue phantom at $\alpha = 45°$ and different directions of the fibre motion and (b) dependence of the incision depth on the tilt angle and the direction of the fibre motion. The mean values and the standard deviations are shown. The power of radiation is $P = 3$ W, the phantom is collagen-free.

same tilt angle moves in the opposite direction, the channel depth is by 20% smaller, and its value is nearly at the same level as in the case of $\alpha = 90°$ (see Fig. 1b). All further experiments were carried out with $\alpha = 45°$.

To study the cutting process in the tissue phantom samples with higher flexibility and elasticity, the samples were prepared with the addition of collagen for stronger resemblance to a soft biological tissue. As seen from Fig. 2, the width of the laser incision d and its depth h depend on the collagen concentration K. When the fibre moves in the direction of the obtuse angle, the depth of the channel is minimal for $K = 10\%$ (Fig. 2a) and the width is maximal for $K = 5\%$ (Fig. 2b). In the case of the fibre moving in the direction of the acute angle, the channel depth monotonically decreases with increasing collagen concentration and is also minimal for $K = 10$ (Fig. 2a); the width of the laser channel is minimal for $K = 5\%$ (Fig. 2b).

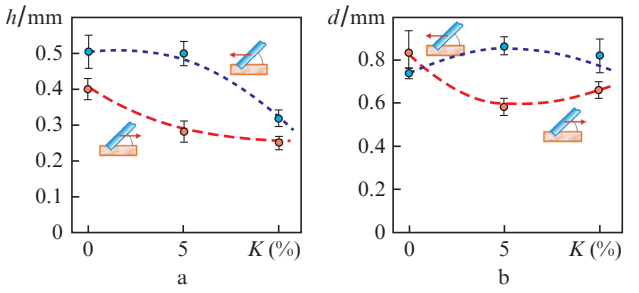

Figure 2. Dependences of the mean values of (a) the laser channel depth h and (b) its width d at the phantom surface on the collagen content. The mean values and the standard deviations are shown, $\alpha = 45°$.

To determine the surface structure of the walls and the bottom of the formed channels the visualisation by means of the scanning electron microscope (SEM) and the luminescence microscope was used in addition to the optical 2D and 3D microscopy. From the SEM image of the segment of laser incision, showing the intact region of the phantom surface, the wall of the channel, and a part of its bottom (Fig. 3a), it follows that the side surface of the channel possesses a pronounced nonuniform relief. The comparison of SEM images in the regions subjected to the laser impact (the bottom of the incision) and the intact region (Fig. 3a) shows that the laser action reduces the small-scale roughness of the phantom surface. The large-scale inhomogeneity of the laser channel bottom is clearly seen in the luminescence image (Fig. 3b), where the strongly luminescent regions of the polymer after the laser impact alternate with the non-luminescent regions (the intact surface of the phantom does not luminesce). The abovementioned large-scale inhomogeneities of the bottom surface of the laser incision are clearly seen in Fig. 3c, obtained using the optical 3D microscope. When the fibre moves in the direction of the obtuse angle, the incision depth is greater than in the case of the opposite direction of motion. The characteristic period of the depth inhomogeneity in this case is also greater.

Figure 4 presents the SEM images of the cleavage of the cartilage tissue phantom along the plane perpendicular to the laser channel. The cross-section of the laser channel (Fig. 4a) is seen to have the shape close to rectangular one. At the side surfaces and the channel bottom the large-scale inhomogeneities can be seen with the characteristic size ~100 μm,

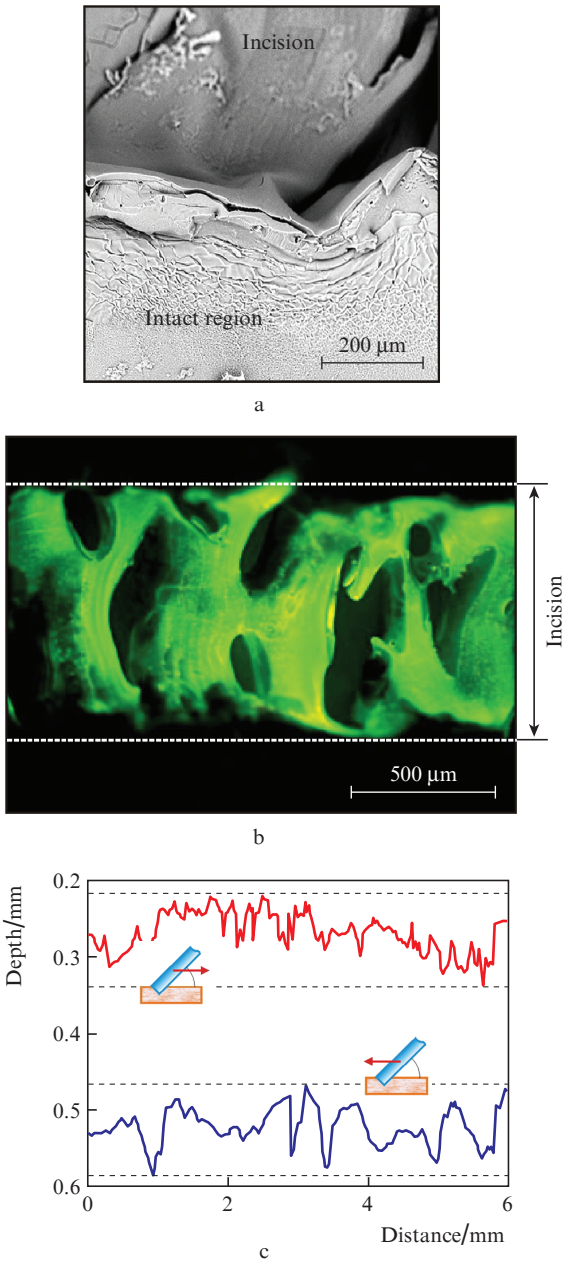

Figure 3. (a) SEM image of the phantom surface with the laser incision, (b) luminescence image of the laser channel bottom and (c) profiles of the channel depth at different directions of the fibre motion. The phantom with 5% collagen content, $\alpha = 45°$.

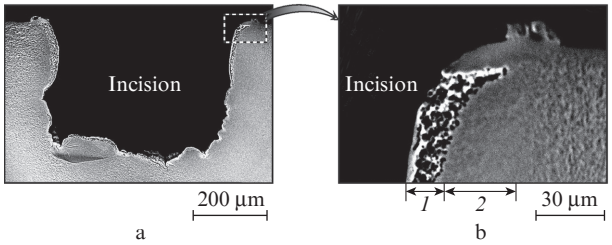

Figure 4. (a) SEM image of the phantom cleavage with the laser incision and (b) magnified image of its edge: (*1*) layer of the porous structure; (*2*) layer with decreased porosity.

and immediately under the channel bottom the structure is highly porous, which is clearly visualised at large magnification (Fig. 4b). The size of the pores of the highly porous structure are in the range from 1 to 10 μm, and the structure thickness amounts to 10–30 μm and is maximal at the walls near the upper edges of the channel. With increasing distance from the channel surface towards the depth of the sample, under the abovementioned highly porous structure, one can observe a layer with the thickness up to 40 μm, which has the porosity lower than that of the intact surface.

Figure 5 presents the results of measuring the maximal temperature near the fibre face, obtained in the process of the laser incision formation at the phantom surface with different directions of the fibre movement and different content of collagen in the sample. As seen from Fig. 5, high temperatures T, exceeding 400 °C, are achieved near the fibre face in the process of phantom cutting. In the case of moving in the direction of the obtuse angle, the measured average temperature is higher ($T = 468 \pm 19$ °C) than that for the movement in the opposite direction ($T = 426 \pm 18$ °C). With increasing collagen concentration in the phantom material (from 0% to 10%) for the movement in the direction of the obtuse angle, a monotonic growth of T is observed. For the opposite direction of the fibre movement, the maximal temperature $T = 450 \pm 3$ °C is achieved at the collagen concentration 5%.

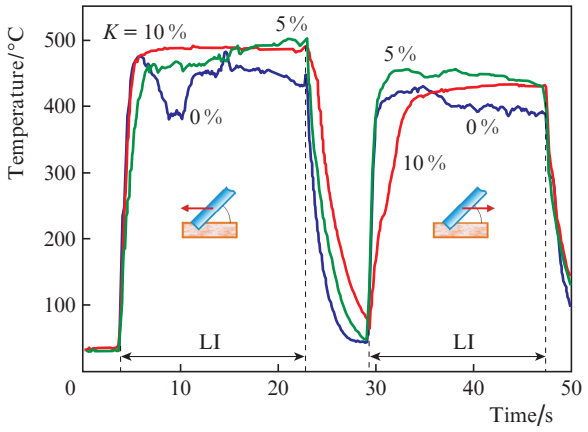

Figure 5. Variations of the maximal temperature values, obtained using the thermal imager camera in the process of laser cutting of the biotissue phantom surface with the different concentrations of collagen hydrolysate in the case of the fibre moving in the direction of the obtuse and the acute angle α. The temporal intervals of the laser operation (LI) are marked.

Figure 6 presents the images of the regions of the glass plate installed at 5 mm from the phantom surface, on which the products of the polymer decomposition in the process of laser cutting of the biotissue phantom are adsorbed in the form of fragments (droplets) having a size from tens to hundreds of micrometres. The thickness of these fragments (Fig. 6b) after evaporation of water does not exceed a few micrometres. In the SEM image one can also clearly see the fragments of the phantom material having micrometre dimensions (marked by arrows in Fig. 6c).

4. Discussion of the results

The performed study of the channel formation process in the biotissue phantoms by means of the fibre laser has shown that the channel parameters, such as the depth, width and surface quality, essentially depend on the tilt angle of the fibre and the direction of its movement (see Fig. 1). For $\alpha \neq 90°$ and the movement of the fibre along the phantom surface in the direction of the obtuse angle the channels are formed with a greater width and depth (see Fig. 1b). The maximal efficiency of the laser cutting is achieved for the tilt angle $\alpha = 45°$ and the fibre moving in the direction of the obtuse angle. Besides that, the main geometric parameters of the laser incision significantly depend on the content of collagen in the biotissue phantom. With increasing collagen concentration, the depth of the produced channel h gradually decreases (Fig. 2a). The value of h depends nonmonotonically on the collagen concentration: both curves demonstrate extrema at $K = 5\%$ (Fig. 2b). At this point one can observe the maximal h, when the fibre moves in the direction of the obtuse angle, and the minimal h for the fibre motion in the opposite direction.

We explain the dependence of the laser incision geometric parameters (depth and width) on the fibre motion direction relative to the biotissue phantom surface by the fact that in the case of moving in the direction of the obtuse angle the fibre face exerts mechanical pressure on a more heated fragment of the phantom than for the opposite direction. Thus, it was recently shown [20] that for a constant force acting on the laser fibre in the direction, parallel to the tissue surface, the nonuniform distribution of temperature near the fibre face monotonically increases the cutting rate with the reduction of the tilt angle from 90° to $\alpha = 45°$ (with the fibre moving in the direction of the obtuse angle).

Our studies with the thermal imaging camera have shown that in the process of the biotissue phantom cutting the temperatures developed near the fibre face exceed 400 °C (see Fig. 5). When the laser is switched on (off), the monotonic

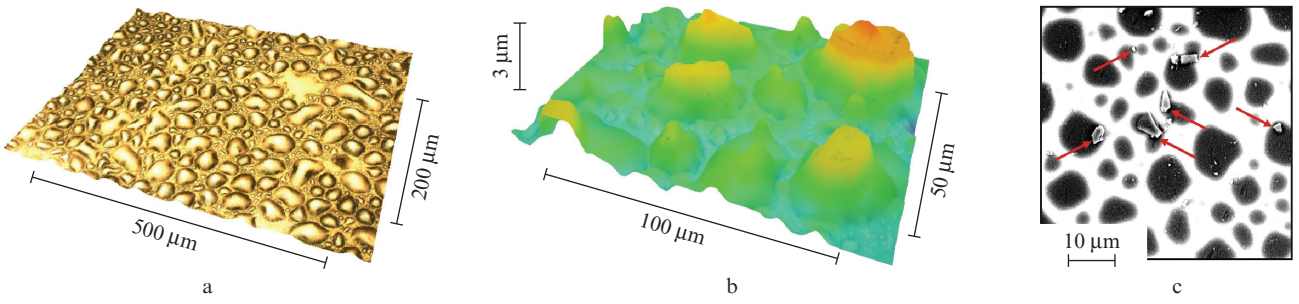

Figure 6. (a, b) 3D images and (c) SEM image of the regions of the glass plate with the products of the polymer decomposition adsorbed in the process of the biotissue phantom laser cutting. The arrows point at the microscopic fragments of the phantom material.

changes of the temperature due to the heating (cooling) of the laser fibre face and the phantom material are observed. This is because the camera records only the thermal radiation with the Planck distribution (the contribution of the laser radiation is absent). Such high values of the temperature can lead not only to the evaporation of water, but also to the destruction of the polymer and even to its carbonisation. The degree of thermal destruction of the material in the general case can be estimated using the damage function $\Omega(r,\tau)$ expressed as the Arrhenius integral [29, 30]:

$$\Omega(r,\tau) = A\int_0^{\tau}\exp\left(-\frac{E_a}{kT(r,t)}\right)dt, \quad (1)$$

where τ is the time of exposure to the high temperature $T(r,t)$ (in K); A is a coefficient; E_a is the activation energy; k is the Boltzmann constant; and t is the time. The function $\Omega(r,\tau)$ characterises the degree of an increase in the number of damages at point r. It shows that the irreversible damages depend not only on the temperature itself, but also on the duration of the temperature action τ. The time of the impact on the phantom tissue can be estimated by the velocity V of the fibre face motion with respect to the phantom surface as $\tau = D/V \approx 0.4$ s, where D is the diameter of the light guiding core of the laser fibre. In the process of the laser incision formation, the exponential dependence of the damaged tissue volume on the temperature T [see Eqn (1)] should lead to a significant change in the removed polymer volume under the small variation of T. This is what we observed in the experiment. Since one can approximate the cross section of the laser-produced incision by a rectangle with the depth h and the width d, the volume of the material removed per unit time amounts to $\sim hdV$. Using the data of Fig. 2 it is easy to find that when the direction of the fibre motion to the obtuse angle changed to the opposite one, the mean temperature decreased by 9% and the mean volume of the removed substance became smaller by 37%.

We believe that the character of the laser-induced impact on the phantom tissue is not restricted to its thermal destruction. It is well known that high and sufficiently fast heating of aqueous solutions and water-containing tissue is always accompanied by the laser-induced hydrodynamic processes, related to the explosive boiling of water with the formation and cavitation collapse of vapour-gas bubbles [12, 23–26, 31, 32]. We also assume that the highly porous structure detected immediately under the surface of the laser channel bottom [layer (*1*) in Fig. 4b] is produced due to heterogeneous explosive boiling in microcavities of the absorber coating of the fibre and the biotissue phantom near the fibre face densely pressed to the tissue [24]. The formation of expanding bubbles in the phantom material in the process of such boiling is implemented according to the thermocavitation mechanism [31–33] and occurs in the closed microscopic volumes [24]. The pressures produced in these volumes under the fast heating of water (1.6 MPa at the temperature 200 °C, and already 4 MPa at 250 °C) lead to the rupture of the tissue phantom, which facilitates the efficient formation of the laser incision with a rate of 1 mm s^{-1}. Such laser-induced shock processes arising near the fibre face under the explosive boiling of water were earlier detected by us using the methods of optoacoustics both in liquid water and in water-saturated tissues in the process of moving the heated fibre face inside them [12, 25, 26].

Because of the inhomogeneity of the absorber coating and the heat removal at the fibre face, the local temperature values at different points of its surface can be somewhat different. However, the mean temperature can be estimated from the specific heat energy flux q (kW cm^{-2}) using the expression [24]:

$$T = T_b + (q + 0.87)/0.04, \quad (2)$$

where T_b is the liquid boiling temperature; $q = P/S$; P is the laser radiation power; and S is the area of the fibre face. For the laser fibre diameter $D = 400$ μm and $P = 3$ W the specific flux is $q \approx 2.4$ kW cm^{-2}, and, according to Eqn (2), for $T_b = 100$ °C at the atmospheric pressure the mean temperature of the face is $T \approx 180$ °C a certain force F, the static pressure $p = F/S$ appears near the face. For $F \approx 0.1$ N the pressure is $p \approx 0.8$ MPa. At this pressure T_b increases to nearly 170 °C and, correspondingly, the mean temperature of the face, according to Eqn (2), will amount already to ~250 °C.

Note that the high static pressure near the laser fibre face, on the one hand, considerably decreases the size of new phase nuclei in the water, and on the other hand, leads to a decrease in the volumes in which the boiling develops. Both factors bring the maximal temperature of the laser heating T to the critical temperature $T_{cr} \approx 374$ °C, and at $T > 0.7T_{cr}$ the explosive boiling arises in water [33], leading to a rupture of the tissue [1, 12, 24].

The same hydrodynamic processes lead to the removal of the fragmented microparticles of the phantom material from the region of laser action near the fibre face. As clearly seen in the SEM image of the glass plate area, such fragments of the phantom material are transported to the distance ~1 cm together with the vapour-gas flows.

Figure 7 presents the schematic illustrating the mechanism of the impact of the moderate-power laser radiation in the process of the incision formation at the biotissue phantom surface.

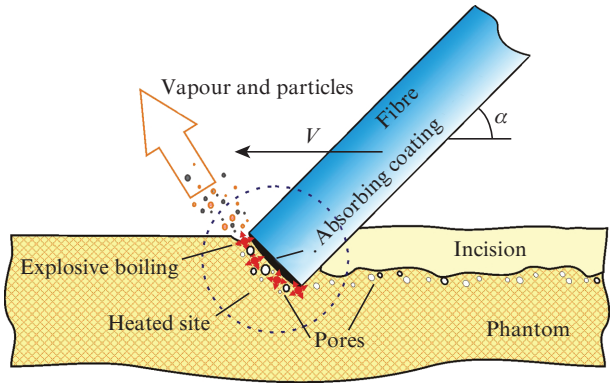

Figure 7. Schematic diagram illustrating the mechanism of the process of biotissue phantom laser cutting with the absorber-coated fibre face.

Under the effect of laser radiation absorbed in the coating, the fibre face is heated to high temperatures exceeding 400 °C (see Fig. 5), and the fibre face becomes a source of broadband IR radiation which is well absorbed in water [1]. Thus, at the temperature of the radiator $T \sim 700$ °C, the maximum of radiation occurs at the wavelength ~3 μm, for which the absorption coefficient in water amounts to 1.1×10^4 cm^{-1} [28]. Since the fibre face in the process of laser cutting is firmly pressed to the phantom tissue, this region of the material also

appears to be significantly heated (the heated region in Fig. 7) due to the heat conduction from the hot face of the fibre. As soon as the laser fibre makes an angle different from 90° with the phantom surface (see Fig. 7) and moves in the direction of the obtuse angle, the face of the fibre mechanically affects the material, heated stronger than for the motion in the opposite direction [17, 20]. This is one of the reasons, why the fibre tilt and direction of the motion affect the geometric parameters of the incision at the phantom surface (Figs 1c, 2 and 3c).

One more factor, causing the dependence of the geometric parameters of the produced incisions on the fibre tilt angle, is due to the laser-induced hydrodynamic processes in water-saturated tissue. Near the face of the fibre, the heating gives rise to heterogeneous explosive boiling of water [24], accompanied by the formation (due to thermocavitation [24]) of expanding vapour-gas bubbles in the water-saturated material of the phantom. Having high inner pressure (above 5×10^6 Pa at $T > 0.7T_{cr}$), these bubbles tear the phantom tissues. Placed in water, such a bubble, according to Ref. [34], would expand to its maximal radius R_{max} and then collapse during the time

$$t = 0.915R_{max}\sqrt{\rho/(p_0 - p_y)}, \quad (3)$$

where ρ is the water density; p_0 is the external pressure (~100 kPa); p_v is the pressure of saturated vapour (2.33 kPa at 20 °C). The vapour bubble with $R_{max} \approx 5$ μm (as in Fig. 4), according to Eqn (3), would collapse during the time $t \approx 0.3$ μs. However, the vapour-gas bubbles that arise in the process of the explosive boiling are surrounded by the heated polymer having high viscosity, which hampers both considerable expansion of the bubbles and their collapse. As a result, near the fibre face (in front of it, as well as near the sidewalls and the bottom of the channel) the highly porous structure is produced (see Fig. 4). It is clear that the permanent generation of such a porous structure near the fibre face will facilitate efficient formation of the incision in the process of moving the fibre ahead (in the direction of obtuse angles).

Note that the presence of a highly porous structure of the polymer subjected to the high-temperature processing near the incision surface is reliably detected by a sharp increase in the luminescence signal from these regions (see Fig. 3b). We believe that the luminescence enhancement at the site of laser impact occurs due to two reasons: 1) a sharp increase in the surface area because of the formation of porous structure; 2) a photothermal rupture of bonds between the polymer molecules accompanied by the formation of double bonds like C=C, etc. [35, 36].

The strong pulsed jumps of pressure (due to the water explosive boiling) and the permanent pressure of the fibre face on the hot modified [4, 7, 37] polymer in the process of the incision formation produce a layer [layer (*1*) in Fig. 4b] with the porosity reduced as compared to that of the intact phantom material [layer (*2*) in Fig. 4b]. This layer underlies the highly porous structure near the incision surface.

Another striking confirmation of the active hydrodynamic processes that occur near the fibre face is the expulsion (together with the vapour-gas flows) of the phantom material microparticles, fragmented by the explosive boiling of water from the site of laser impact (Fig. 6c).

We have shown that in the case of using the optical fibre with absorbing coating, the laser incisions are mainly formed at the expense of the primary heating of the fibre face, while the effect of the laser radiation itself is minimal. The cutting process itself occurs mainly due to the heat transfer, the generation of broad-band IR radiation by the hot fibre face, and the laser-induced hydrodynamic processes. In spite of these facts, following the terminology commonly accepted in medicine, the studied process is referred to as laser cutting.

5. Conclusions

We have studied the thermal and transport processes that occur in the course of the laser incision formation at the surface of a biological tissue phantom. The cutting is implemented using the face of an optical fibre with and absorbing coating, heated with the continuous-wave laser radiation at $\lambda = 1.94$ μm. Such processes occur in some clinical procedures, related to the biotissue dissection and removal.

We have studied the dependences of the geometric parameters of the incision, produced by the optical fibre moving with the velocity 1 mm s^{-1}, on the tilt angle of the fibre and the direction of its motion relative to the phantom surface. We have found that when the fibre moves in the direction of the obtuse angle, the incision depth monotonically increases with decreasing fibre tilt angle from 90° to 45°. Alongside with the purely thermal action of the laser radiation, the laser-induced hydrodynamic processes due to water explosive boiling are shown to cause the effect. Such processes lead not only to the tissue rupture near the fibre face with the partial ejection of the fragmented substance from the site of laser impact, but also to the formation of a highly porous structure in the immediate vicinity of the fibre face and near the incision surface.

Acknowledgements. The authors thank A.P. Sviridov for useful advice on the synthesis of the biological tissue phantom and N.V. Minaev for the help in designing the setup.

The work was partially supported by the Russian Science Foundation (Grant No. 14-15-00840) in the part concerning the studies of thermal laser-induced processes and by the Russian Foundation for Basic Research (Grant No. 17-02-00832) in the part related to the study of hydrodynamic and transport processes.

References

1. Skobelkin O.K. (Ed.) *Lazery v khirurgii* (Lasers in Surgery) (Moscow: Meditsina, 1989).
2. Waynant R.W. (Ed.) *Lasers In Medicine* (Boca Raton, FL: CRC press, 2001).
3. Sandler B.I., Sulyandziga L.N., Chudnovskii V.M., Yusupov V.I., et al. *Perspektivy lecheniya diskogennykh kompressionnykh form poyasnichno-kresttsovykh radikulitov s pomoshchyu punktsionnykh neendoskopicheskikh lasernykh operatsii* (Prospects of Treatment of Discogenic Compression Forms of Lumbosacral Radiculitis by Paracentetic Non-Endoscopic Laser Operations) (Vladivostok: Dal'nauka, 2004) p. 181.
4. Bagratashvili V.N., Sobol' E.N., Shekhter A.B. *Lazernaya inzheneriya khryashchey* (Laser Engineering of Cartilages) (Moscow: Fizmatlit, 2006).
5. Peng Q., Juzeniene A., Chen J., Svaasand L.O., Warloe T., Giercksky K.E., Moan J. *Lasers Med. Rep. Prog. Phys.*, **71** (5), 056701 (2008).
6. Welch A.J., Van Gemert M.J. (Eds) *Optical-Thermal Response of Laser-Irradiated Tissue* (Berlin: Springer, 2011) Vol. 2.
7. Bagratashvili V.N., Lunin V.V., Zakharkina O.L., Ignatyeva N.Yu. *Lazero-indutsirovannaya i termicheskaya modifikatsiya struktury soyedinitel'nykh tkaney* (Laser-induced and Thermal Modification of the Connective Tissue Structure) (Moscow: Intellekt, 2016).
8. Minaev V.P. *Almanakh Klinicheskoi Meditsiny*, **17** (2), 116 (2008).
9. Woods S., Duka M., Flinn G. *Fotonika*, **4**, 6 (2008).

10. Minaev V.P. *Lazernye meditsinskiye sistemy i meditsinskiye tekhnologii na ikh osnove. Uchebnoye posobiye* (Laser Medical Systems and Medical Technologies Based on Them. A Tutorial) (Dolgoprudnyi: Intellekt, 2017).
11. Krochek I.V., Privalov V.A., Lappa A.V., Evnevich M.V., Minaev V.P. *Lazernaya osteoperforatsiya v lechenii ostrogo i khronicheskogo osteomielita. Metodicheskiye rekomendatsii* (Laser Osteoperforation in the Treatment of Acute and Chronic Osteomyelitis. Methodical Recommendations) (Chelyabinsk: ChGMA, ChGU, 2004).
12. Yusupov V.I., Chudnovskii V.M., Bagratashvili V.N., in *Hydrodynamics – Advanced Topics* (Rijeka, Croatia: InTech, 2011) pp 95–118.
13. Bredikhin V., Kamensky V., Sapogova N., Elagin V., Shakhova M., Biturin N. *Appl. Phys. A*, **122** (3), 104 (2016).
14. Romanos G.E. *Compendium of Continuing Education in Dentistry*, **34** (10), 752 (2013).
15. Yusupov V.I., Chudnovskii V.M., Bagratashvili V.N. *Laser Phys.*, **21** (7), 1230 (2011).
16. Kamalski D.M., de Boorder T., Bittermann A.J., Wegner I., Vincent R., Grolman W. *Otology & Neurotology*, **35** (6), 1070 (2014).
17. Chudnovskii V.M., Yusupov V.I. Patent of the Russian Federation No. 103302 (2011).
18. Belikov A.V., Skripnik A.V., Kurnyshev V.Yu., Shatilova K.V. *Quantum Electron.*, **46** (6), 534 (2016) [*Kvantovaya Elektron.*, **46** (6), 534 (2016)].
19. Skripnik A.V. *Izv. Vyssh. Uchebn. Zaved., Ser. Priborostr.*, **56**, 37 (2013).
20. Sapogova N., Bredikhin V., Bityurin N., Kamensky V., Zhigarcov V., Yusupov V. *Biomed. Opt. Express*, **8** (1), 104 (2017).
21. Proebstle T.M., Lehr H.A., Kargl A., Espinola-Klein C., Rother W., Bethge S., Knop J. *J. Vascular Surg.*, **35** (4), 729 (2002).
22. Chudnovskii V.M., Yusupov V.I., Zakharkina O.L., Ignatyeva N.Yu., Zhigar'kov V.S., Yashkin M.N., Bagratashvili V.N. *Sovrem. Tekhnol. Med.*, **8** (2), 6 (2016).
23. Chudnovskii V.M., Yusupov V.I., Zhukov S.A., Echmaev S.B., Bagratashvili V.N. *Doklady Physics*, **62** (4), 174 (2017) [*Dokl. Akad. Nauk*, **473** (5), 533 (2017)].
24. Chudnovskii V.M., Yusupov V.I., Dydyrin A.V., Nevozhay V.I, Kisilev A.Yu., Zhukov S.A., Bagratashvili V.N. *Quantum Elecron.*, **47** (4), 361 (2017) [*Kvantovaya Elektron.*, **47** (4), 361 (2017)].
25. Yusupov V.I., Konovalov A.N., Ulyanov V.A., Bagratashvili V.N. *Acoustical Physics*, **62** (5), 537 (2016) [*Akust. Zh.*, **62** (5), 531 (2016)].
26. Yusupov V.I., Bulanov V.V., Chudnovskii V.M., Bagratashvili V.N. *Laser Phys.*, **24** (1), 015601 (2014).
27. Kondyurin A.V., Sviridov A.P. *Quantum Electron.*, **38** (7), 641 (2008) [*Kvantovaya Elektron.*, **38** (7), 641 (2008)].
28. Hale G.M., Querry M.R. *Appl. Opt.*, **12** (3), 555 (1973).
29. Pearce J.A., in *SPIE BiOS: Biomed. Opt.*, **7181**, 718104 (2009).
30. Mignon C., Rodriguez A.H., Palero J.A., Varghese B., Jurna M. *Biomed. Opt. Express*, **7** (12), 4974 (2016).
31. Rastopov S.F., Sukhodolsky A.T. *Phys. Lett. A*, **149**, 229 (1990).
32. Padilla-Martinez J.P., Berrospe-Rodriguez C., Aguilar G., Ramirez-San-Juan J.C., Ramos-Garcia R. *Phys. Fluids*, **26**, 122007 (2014).
33. Skripov V.P., Sinitsyn E.N., Pavlov P.A., Ermakov G.V., Muratov G.N., Bulanov N.V., Baidakov V.G. *Thermophysical Properties of Liquids in the Metastable (Superheated) State* (New York: Gordon and Breach Sci. Publ., 1988).
34. Keller J.B., Miksis M. *J. Acoust. Soc. Am.*, **68** (2), 628 (1980).
35. Zapol'skii O.B. *Polymer Science USSR*, **7**, 678 (1965) [*Vysokomol. Soed.*, **7** (4), 615 (1965)].
36. Beyler C.L., Hirschler M.M. *SFPE Handbook of Fire Protection Engineering*, **2**, 111 (2002).
37. Antonov E.N., Krotova L.I., Minaev N.V., Minaeva S.A., Mironov A.V., Popov V.K., Bagratashvili V.N. *Quantum Electron.*, **45** (11), 1023 (2015) [*Kvantovaya Elektron.*, **45** (11), 1023 (2015)].